

# A FINITE ELEMENT METHOD FOR THE SIMULTANEOUS ANALYSIS OF IMPLICITLY DEFINED REISSNER–MINDLIN SHELLS

MICHAEL W. KAISER<sup>1,2</sup>, THOMAS-PETER FRIES<sup>1,3</sup>

<sup>1</sup> Institute of Structural Analysis  
Graz University of Technology  
Lessingstr. 25, 8010 Graz, Austria  
www.ifb.tugraz.at

<sup>2</sup> email: michael.kaiser@tugraz.at

<sup>3</sup> email: fries@tugraz.at

**Key words:** Fictitious domain methods, FEM, level-set method, shells, curved beams

**Summary.** We present a method to solve *simultaneously* all Reissner–Mindlin shells which are embedded in a three-dimensional bulk domain. The shells are described by level sets of a level-set function, hence, a coordinate-free formulation of the shell model which is valid for an implicit geometry definition is required. The presented finite element method (FEM) is a hybrid between the classical FEM and a fictitious domain method. Therefore, it was previously coined Bulk Trace FEM. Numerical results confirm higher-order convergence rates.

## 1 INTRODUCTION

Shells are common structures in nature and engineering. Usually, one specific shell geometry is analysed in the design process, i.e., the geometry of this shell is described and the mechanical quantities, e.g., deformations, stresses, and energies are computed. Mostly, the analysis is based on a geometry description and formulation of differential operators in curvilinear coordinates and, therefore, a parametrization of the geometry is required [1, 2]. Furthermore, the shell model can be stated in a coordinate-free formulation which is valid for geometries that are given explicitly, e.g., by a parametrization or implicitly, e.g., by a level set of a level-set function. In [3] the Kirchhoff-Love shell model has been reformulated in a coordinate free-formulation and the Reissner–Mindlin shell model in [4]. Analogously, such coordinate-free formulations can be obtained for beams, e.g., [5, 6] and for geometrically non-linear ropes and membranes, c.f., [7]. Differential operators in these models are formulated using the Tangential Differential Calculus (TDC), c.f., [8]. If one single shell geometry is given implicitly, the Trace FEM can be used for the analysis, e.g., [9] for Reissner–Mindlin shells.

In this work, we present a mechanical model and finite element method for the *simultaneous solution* of all Reissner–Mindlin shells which are embedded in a three-dimensional bulk domain. The individual middle surfaces of the shells are level sets  $\Gamma^c$  of a level-set function  $\phi$ , hence, the geometry of the shell is described implicitly and a coordinate-free formulation of the governing equations, c.f., [4] is required. Furthermore, the co-area formula is used to formulate the weak

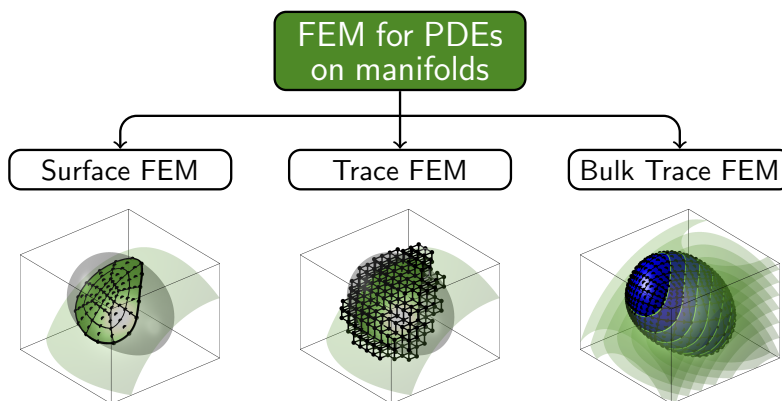


Figure 1: Different FEM approaches for PDEs on manifolds.

form. Applications for this approach might be in the design process to find certain geometries with desired target properties in a family of possible geometries or to use shells as reinforcement structures in new anisotropic material models. For more detailed discussions, we refer to our previous publication [10]. For the lower-dimensional case, i.e., when a one-dimensional structure is embedded in a two-dimensional bulk domain, an analogous model for Timoshenko beams follows, c.f., [11]. In the context of transport problems, the simultaneous solution for all embedded  $d$ -dimensional structures in a  $(d + 1)$ -dimensional space is shown, e.g., in [12, 13]. For the simultaneous solution of geometrically non-linear ropes and membranes, we refer to our works in [14, 15, 16].

Different approaches may be distinguished to solve PDEs on manifolds using the finite element method. In the context of Reissner–Mindlin shells, as in this paper, the manifold is the shell’s middle surface but generally the manifold may be some curved surface or line on which some physical process occurs. One possibility is to approximate the solution for *one* geometry by the classical Surface FEM based on a parametrization of the manifold. Then, the geometry of interest is represented by a conforming mesh composed by curved (surface or line) elements. Furthermore, fictitious domain methods, e.g., the Trace FEM, might be used. Therein, *one* manifold of interest with dimension  $d$  is embedded in a  $(d + 1)$ -dimensional background mesh. For the numerical analysis, only the elements which are cut by the manifold are considered. This often requires special attention, e.g., in the context of stabilization and the enforcement of (essential) boundary conditions because the boundary is usually no longer conforming. The approach used in this paper, previously labelled Bulk Trace FEM in [14], can be seen as a hybrid between the Surface FEM and the Trace FEM for the *simultaneous* analysis of *many* geometries at once. The mesh is by no means aligned to the level sets which are embedded in the bulk domain but the boundary is conforming. Therefore, no stabilization is required and boundary conditions are enforced strongly as in the surface FEM. Fig. 1 compares these three different FEM approaches.

The remainder of this paper is as follows: In Section 2, the definition of the geometric setup and the required differential operators are introduced. The mechanical model is derived in Section 3 and posed in the weak form, to be used in the finite element method as described in Section 4. Numerical results to verify the new methodology follow in Section 5. The paper

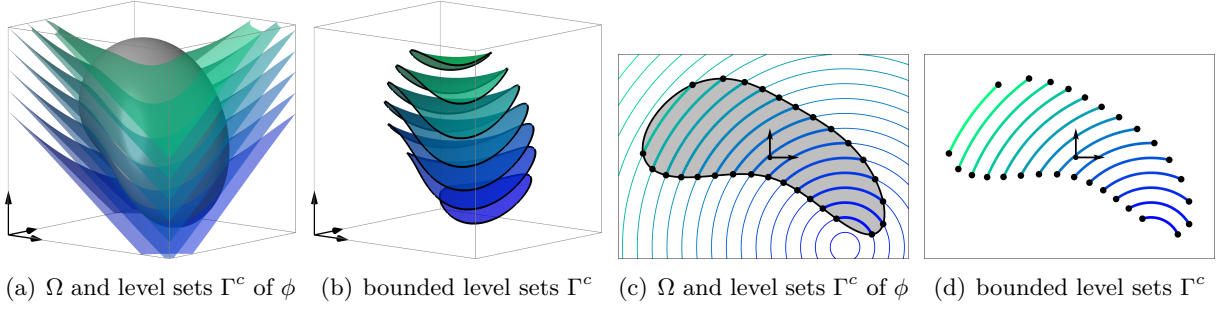


Figure 2: Some bulk domain  $\Omega$ , level-set function  $\phi(\mathbf{x})$ , and implied level sets  $\Gamma^c$ . (a) and (b) show the situation for shells, (c) and (d) for beams.

closes in Section 6, including an outlook to further research.

## 2 GEOMETRY REPRESENTATION AND DIFFERENTIAL OPERATORS

The shell is modelled by its middle surface which is a manifold of co-dimension 1 and implicitly described as the level set  $\Gamma^c$  of a scalar level set function  $\phi(\mathbf{x}) : \Omega \rightarrow \mathbb{R}$  where  $c$  is a constant level-set value.  $\Omega$  is the bulk domain, i.e.,  $\Omega \subset \mathbb{R}^3$  for shells and  $\Omega \subset \mathbb{R}^2$  for beams. Within the bulk domain, a minimum value  $\phi^{\min} = \inf \phi$  and a maximum value  $\phi^{\max} = \sup \phi$  of the level-set function is defined. Furthermore, the bulk domain can be specified by prescribed values for  $\phi^{\min}$  and  $\phi^{\max}$ . In the following, all level sets, i.e., shells, which are embedded in the bulk domain are considered simultaneously. These are

$$\Gamma^c = \{\mathbf{x} \in \Omega : \phi(\mathbf{x}) = c \in \mathbb{R}\}, \phi^{\min} < c < \phi^{\max}. \quad (1)$$

Fig. 2 shows the situation for shells and beams. For a more detailed discussion, including requirements for valid combinations of bulk domains and level-set functions, the reader is referred to [11, 14].

To formulate the differential operators and divergence theorems used in the formulation of the strong and weak form of the governing equations, some vector fields are required:

- Normal vectors to the boundary of the bulk domain:  $\mathbf{m}(\mathbf{x})$ ,  $\mathbf{x} \in \partial\Omega$ . The definition of these vectors depends on how the bulk domain is described (explicitly or implicitly). However, it is a standard task in the FEM to obtain such normal vectors based on existing meshes (here: of the bulk domain), therefore, these are not further specified here.
- Normal vectors:  $\mathbf{n}(\mathbf{x}) = \frac{\mathbf{n}^*}{\|\mathbf{n}^*\|}$  with  $\mathbf{n}^* = \nabla\phi(\mathbf{x})$ ,  $\mathbf{x} \in \Omega$ .
- Tangential vectors:  $\mathbf{t} = \mathbf{m} \times \mathbf{n}$ .
- Co-normal vectors:  $\mathbf{q}(\mathbf{x}) = \frac{\mathbf{q}^*}{\|\mathbf{q}^*\|}$  with  $\mathbf{q}^* = \mathbf{n} \times \mathbf{t}$ .

These vectors are visualized for one selected manifold in Fig. 3. With the normal vector and the  $(d \times d)$ -identity matrix, the projector onto the tangent space is defined as

$$\mathbf{P} = \mathbf{I} - \mathbf{n} \otimes \mathbf{n} = \mathbf{I} - \mathbf{Q}. \quad (2)$$

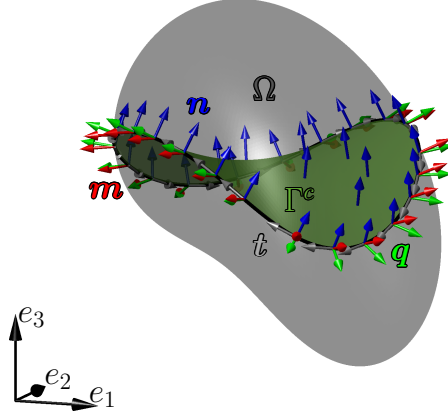


Figure 3: Normal vector field  $\mathbf{n}$  living on the manifold  $\Gamma^c$  and along the boundary  $\partial\Gamma^c$  depicted in blue, vector fields  $\mathbf{t}$  depicted in grey and  $\mathbf{q}$  depicted in green on the boundary of the manifold  $\partial\Gamma^c$ , and normal vector field  $\mathbf{m}$  to the boundary of the bulk domain  $\partial\Omega$ . Note that for clarity, only one surface is shown but the situation applies to every embedded level set  $\Gamma^c$  in  $\Omega$ .

Furthermore, *tangential* or *surface* differential operators are defined. These are used in the formulation of the governing equations.  $\nabla\bullet$  is the classical gradient w.r.t. the bulk domain, i.e., the three-dimensional space  $\mathbb{R}^3$  for shells. Then, for the tangential gradient of a scalar function  $f$  follows

$$\nabla_{\Gamma} f = \mathbf{P} \cdot \nabla f. \quad (3)$$

For the surface gradient of a vector-valued function  $\mathbf{v}$  a *directional* and a *covariant* surface gradient have to be distinguished. These are defined as

$$\nabla_{\Gamma}^{\text{dir}} \mathbf{v} = \nabla \mathbf{v} \cdot \mathbf{P} \quad \text{and} \quad \nabla_{\Gamma}^{\text{cov}} \mathbf{v} = \mathbf{P} \cdot \nabla_{\Gamma}^{\text{dir}} \mathbf{v} = \mathbf{P} \cdot \nabla \mathbf{v} \cdot \mathbf{P}. \quad (4)$$

Note that  $\nabla_{\Gamma}^{\text{dir}} \mathbf{v}$  is generally not in the tangent space of the manifold while  $\nabla_{\Gamma}^{\text{cov}} \mathbf{v}$  is. The divergence of a vector-valued function is given by

$$\text{div}_{\Gamma} \mathbf{v} = \text{tr}(\nabla_{\Gamma}^{\text{dir}} \mathbf{v}) = \text{tr}(\nabla_{\Gamma}^{\text{cov}} \mathbf{v}) = \nabla_{\Gamma} \cdot \mathbf{v} \quad (5)$$

and, for a second-order tensor function  $\mathbf{T}$ , the divergence is determined by

$$\text{div}_{\Gamma} \mathbf{T} = \begin{bmatrix} \text{div}_{\Gamma} (T_{11}, T_{12}, T_{13}) \\ \text{div}_{\Gamma} (T_{21}, T_{22}, T_{23}) \\ \text{div}_{\Gamma} (T_{31}, T_{32}, T_{33}) \end{bmatrix} = \nabla_{\Gamma} \cdot \mathbf{T}. \quad (6)$$

Another important quantity is curvature. In the context of the TDC, it is defined based on the Weingarten map, that is

$$\mathbf{H} = \nabla_{\Gamma}^{\text{dir}} \mathbf{n} = \nabla_{\Gamma}^{\text{cov}} \mathbf{n}. \quad (7)$$

The mean curvature is defined as

$$\varkappa = \text{tr}(\mathbf{H}) = \text{div}_{\Gamma} \mathbf{n}. \quad (8)$$

The divergence theorem for a vector-valued function  $\mathbf{v}$  and for a second-order tensor-valued function  $\mathbf{T}$  on a *single* surface  $\Gamma^c$ , defined by *one* constant value for  $c$ , is [3]

$$\int_{\Gamma^c} \mathbf{v} \cdot \operatorname{div}_{\Gamma} \mathbf{T} \, d\Gamma = - \int_{\Gamma^c} \nabla_{\Gamma}^{\operatorname{dir}} \mathbf{v} : \mathbf{T} \, d\Gamma + \int_{\Gamma^c} \varkappa \cdot \mathbf{v} \cdot (\mathbf{T} \cdot \mathbf{n}) \, d\Gamma + \int_{\partial\Gamma^c} \mathbf{v} \cdot (\mathbf{T} \cdot \mathbf{q}) \, d\partial\Gamma, \quad (9)$$

For the simultaneous solution of all embedded shells, the co-area formula [13, 12, 14] is required. It is defined as

$$\int_{\phi^{\min}}^{\phi^{\max}} \int_{\Gamma^c} f \, d\Gamma \, dc = \int_{\Omega} f \cdot \|\nabla\phi\| \, d\Omega \quad (10)$$

in the domain and at the boundary as

$$\int_{\phi^{\min}}^{\phi^{\max}} \int_{\partial\Gamma^c} f \cdot \mathbf{q} \, d\partial\Gamma \, dc = \int_{\Omega} f \cdot \mathbf{q} \cdot (\mathbf{q} \cdot \mathbf{m}) \cdot \|\nabla\phi\| \, d\partial\Omega. \quad (11)$$

With Eqs. (10) and (11) the divergence theorem in Eq. (9) is extended to

$$\begin{aligned} \int_{\Omega} \mathbf{v} \cdot \operatorname{div}_{\Gamma} \mathbf{T} \cdot \|\nabla\phi\| \, d\Omega &= - \int_{\Omega} \nabla_{\Gamma}^{\operatorname{dir}} \mathbf{v} : \mathbf{T} \cdot \|\nabla\phi\| \, d\Omega + \int_{\Omega} \varkappa \cdot \mathbf{v} \cdot (\mathbf{T} \cdot \mathbf{n}) \cdot \|\nabla\phi\| \, d\Omega \\ &+ \int_{\partial\Omega} \mathbf{v} \cdot (\mathbf{T} \cdot \mathbf{q}) \cdot (\mathbf{q} \cdot \mathbf{m}) \cdot \|\nabla\phi\| \, d\partial\Omega. \end{aligned} \quad (12)$$

Note that the term with the mean curvature  $\varkappa$  vanishes for in-plane tensors.

### 3 MECHANICAL MODEL

The coordinate-free definition of the governing equations and their derivation for the case of *one* shell geometry is given in detail in [3] and further in [4, 10]. Therefore, we summarize it in this paper in a short and concise manner and refer to the aforementioned literature for further details. Fig. 4 shows the situation of the kinematic relations for *many* embedded Reissner–Mindlin shells and for the situation of *one single* shell. The displacement is defined as

$$\mathbf{u}_{\hat{\Omega}^c}(\mathbf{x}) = \mathbf{u}_{\hat{\Omega}^c}(\mathbf{x}_{\Gamma}, \zeta) = \mathbf{u}(\mathbf{x}_{\Gamma}) + \zeta \mathbf{w}(\mathbf{x}_{\Gamma}), \quad (13)$$

with the displacement of the mid-surface  $\mathbf{u}(\mathbf{x}_{\Gamma})$  and the difference vector  $\mathbf{w}(\mathbf{x}_{\Gamma})$  which describes the rotation of the shell director (normal),  $\gamma$  is the transverse shear deformation, and  $\zeta \leq |\frac{t}{2}|$  describes the shell thickness. The membrane, bending, and transverse shear strain tensors are defined as

$$\boldsymbol{\varepsilon}_{\Gamma, \operatorname{Memb}}^{\operatorname{P}}(\mathbf{u}) = \frac{1}{2} \left[ \nabla_{\Gamma}^{\operatorname{cov}} \mathbf{u} + (\nabla_{\Gamma}^{\operatorname{cov}} \mathbf{u})^{\operatorname{T}} \right], \quad (14)$$

$$\boldsymbol{\varepsilon}_{\Gamma, \operatorname{Bend}}^{\operatorname{P}}(\mathbf{u}, \mathbf{w}) = \frac{1}{2} \left[ \mathbf{H} \cdot \nabla_{\Gamma}^{\operatorname{dir}} \mathbf{u} + \left( \nabla_{\Gamma}^{\operatorname{dir}} \mathbf{u} \right)^{\operatorname{T}} \cdot \mathbf{H} + \nabla_{\Gamma}^{\operatorname{cov}} \mathbf{w} + (\nabla_{\Gamma}^{\operatorname{cov}} \mathbf{w})^{\operatorname{T}} \right], \quad (15)$$

$$\boldsymbol{\varepsilon}_{\Gamma}^{\operatorname{S}}(\mathbf{u}, \mathbf{w}) = \frac{1}{2} \left[ \mathbf{Q} \cdot \nabla_{\Gamma}^{\operatorname{dir}} \mathbf{u} + \left( \nabla_{\Gamma}^{\operatorname{dir}} \mathbf{u} \right)^{\operatorname{T}} \cdot \mathbf{Q} + \mathbf{n} \otimes \mathbf{w} + \mathbf{w} \otimes \mathbf{n} \right], \quad (16)$$

The constitutive law for a linear elastic material with Lamé constants  $\lambda$  and  $\mu$  for plane stress leads to the stress tensor

$$\boldsymbol{\sigma}_{\Gamma}(\mathbf{x}) = 2\mu \boldsymbol{\varepsilon}_{\Gamma}(\mathbf{x}) + \lambda \operatorname{tr}[\boldsymbol{\varepsilon}_{\Gamma}(\mathbf{x})] \mathbf{I}. \quad (17)$$

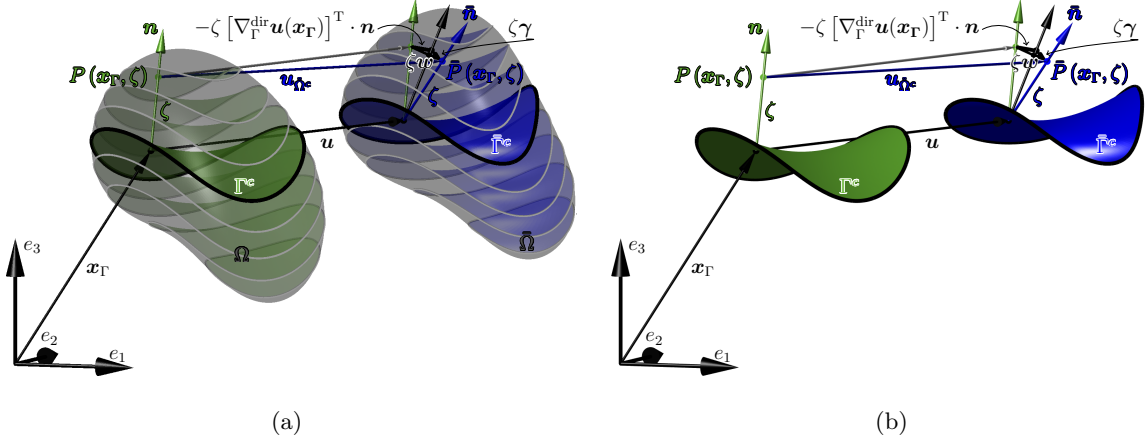


Figure 4: The shell kinematics for (a) some shells embedded in the bulk domain and (b) a single shell.

For the bending moment tensor  $\mathbf{m}_\Gamma$ , the effective normal force tensor  $\tilde{\mathbf{n}}_\Gamma$  and the transverse shear force tensor  $\mathbf{q}_\Gamma$  follows:

$$\mathbf{m}_\Gamma = \int_{-t/2}^{t/2} \zeta \mathbf{P} \cdot \boldsymbol{\sigma}_\Gamma \cdot \mathbf{P} \, d\zeta = \frac{t^3}{12} \boldsymbol{\sigma}_\Gamma^P (\boldsymbol{\varepsilon}_{\Gamma, \text{Bend}}^P), \quad (18)$$

$$\tilde{\mathbf{n}}_\Gamma = \int_{-t/2}^{t/2} \mathbf{P} \cdot \boldsymbol{\sigma}_\Gamma \cdot \mathbf{P} \, d\zeta = t \boldsymbol{\sigma}_\Gamma^P (\boldsymbol{\varepsilon}_{\Gamma, \text{Membr}}^P), \quad (19)$$

$$\mathbf{q}_\Gamma = \int_{-t/2}^{t/2} \mathbf{Q} \cdot \boldsymbol{\sigma}_\Gamma + \boldsymbol{\sigma}_\Gamma \cdot \mathbf{Q} \, d\zeta = t \boldsymbol{\sigma}_\Gamma^S (\boldsymbol{\varepsilon}_\Gamma^S) = 2t\mu\alpha_s \boldsymbol{\varepsilon}_\Gamma^S. \quad (20)$$

Note that for  $\mathbf{q}_\Gamma$ , a shear correction factor  $\alpha_s$  is considered and that the real normal force tensor is defined as  $\mathbf{n}_\Gamma^{\text{real}} = \tilde{\mathbf{n}}_\Gamma + \mathbf{H} \cdot \mathbf{m}_\Gamma$ .

With Eqs. (13) to (20), there follows the Reissner–Mindlin shell model in strong form as

$$\text{div}_\Gamma \mathbf{n}_\Gamma^{\text{real}} + \mathbf{Q} \cdot \text{div}_\Gamma \mathbf{q}_\Gamma + \mathbf{H} \cdot (\mathbf{q}_\Gamma \cdot \mathbf{n}) = -\mathbf{f}, \quad (21)$$

$$\mathbf{P} \cdot \text{div}_\Gamma \mathbf{m}_\Gamma - \mathbf{q}_\Gamma \cdot \mathbf{n} = -\mathbf{c}. \quad (22)$$

$\mathbf{f}$  is the applied load vector per area and  $\mathbf{c}$  is the applied moment vector. The boundary value problem (BVP) is completed by sufficient boundary conditions. Note that in this BVP quantities with index  $\Gamma$  are tensors, e.g., the shear force tensor  $\mathbf{q}_\Gamma$ , while the quantities without the index are vectors, e.g., the co-normal vector  $\mathbf{q}$ . Furthermore, note that for Timoshenko beams, the governing equations have formally a very similar structure. This is because the Timoshenko beam model is a dimensional reduction of the Reissner–Mindlin shell model. The differences are the dimensions and the definition of the tensors of the internal moment and forces, see, e.g., [11].

#### 4 WEAK FORM AND NUMERICAL ANALYSIS

To obtain the weak form of the governing equations, which are required for the FEM analysis, Eq. (21) is multiplied with the test functions  $\mathbf{v}_u$  and Eq. (22) is multiplied with the test functions

$\mathbf{v}_w$ . Then, the divergence theorem, Eq. (9), is applied which leads to *domain* integrals  $\int_{\Gamma^c} \bullet \, d\Gamma$  and *boundary* integrals  $\int_{\partial\Gamma^c} \bullet \cdot \mathbf{q} \, d\partial\Gamma$ . An integration over *all* level sets embedded in the bulk domain leads to  $\int \int_{\Gamma^c} \bullet \, d\Gamma \, dc$  and  $\int \int_{\partial\Gamma^c} \bullet \cdot \mathbf{q} \, d\partial\Gamma \, dc$ . Finally the co-area formulas, Eqs. (10) and (11), are applied, respectively. This leads to the continuous weak form, formulated over the bulk domain. Only first derivatives occur and, therefore, standard Lagrange-type finite elements can be used. For more details about the continuous weak form and the corresponding function spaces, we refer to [10].

The discrete weak form is obtained by discretizing the bulk domain with  $C^0$ -continuous Lagrange-type elements. It should again be emphasized that the mesh does by no means have to align with the level sets in the bulk domain. The difference vector is an in-plane quantity. In the FEM, this can be enforced by the tangentiality constraint  $\mathbf{w}^h \cdot \mathbf{n} = 0$ , used with a Lagrange multiplier or by projecting the difference vector onto the tangent space as  $\mathbf{w}^h = \mathbf{P} \cdot \check{\mathbf{w}}^h$ .  $\check{\bullet}$  is a (general) vector, defined in  $\mathbb{R}^3$ , i.e., it is not (necessarily) tangential to the manifold. The second variant is used in this paper. Therefore, also the test function  $\mathbf{v}_w^h = \mathbf{P} \cdot \check{\mathbf{v}}_w^h$  must be projected and the penalty term  $\rho_w (\check{\mathbf{w}}^h \cdot \mathbf{n}) (\check{\mathbf{v}}_w^h \cdot \mathbf{n})$  is added in Eq. (24). The penalty parameter is  $\rho_w = E \cdot t$ , with Young's modulus  $E$  and the shell's thickness  $t$ . Further discussions about the tangentiality constraint of the difference vector and how it can be considered in the FEM, are found in [10, 4, 9]. Finally, the discrete weak form reads: With the given material parameters  $E \in \mathbb{R}^+$ ,  $\nu \in [0, 0.5)$ , body forces  $\mathbf{f} \in \mathbb{R}^3$  on  $\Gamma^c$ , tractions  $\hat{\mathbf{p}}_{\partial\Gamma}$  on  $\partial\Gamma_{N,u}^c$ , find  $\mathbf{u} \in \mathcal{S}_u$  and  $\mathbf{w} \in \mathcal{S}_w$  such that for all  $\mathbf{v}_u \in \mathcal{V}_u$  and for all  $\mathbf{v}_w \in \mathcal{V}_w$ , there holds

$$\int_{\Omega^h} \left[ \nabla_{\Gamma}^{\text{dir}} \mathbf{v}_u^h : \tilde{\mathbf{n}}_{\Gamma} + \left( \mathbf{H} \cdot \nabla_{\Gamma}^{\text{dir}} \mathbf{v}_u^h \right) : \mathbf{m}_{\Gamma} + \left( \mathbf{Q} \cdot \nabla_{\Gamma}^{\text{dir}} \mathbf{v}_u^h \right) : \mathbf{q}_{\Gamma} \right] \cdot \|\nabla\phi^h\| \, d\Omega = \int_{\Omega^h} \mathbf{v}_u^h \cdot \mathbf{f} \cdot \|\nabla\phi^h\| \, d\Omega + \int_{\partial\Omega_{N,u}^h} \mathbf{v}_u^h \cdot \hat{\mathbf{p}}_{\partial\Gamma} \cdot (\mathbf{q} \cdot \mathbf{m}) \cdot \|\nabla\phi^h\| \, d\partial\Omega, \quad (23)$$

$$\int_{\Omega^h} \left( \nabla_{\Gamma}^{\text{dir}} \mathbf{v}_w^h : \mathbf{m}_{\Gamma} + \mathbf{v}_w^h \cdot \mathbf{q}_{\Gamma} \cdot \mathbf{n} + \rho_w (\check{\mathbf{w}}^h \cdot \mathbf{n}) (\check{\mathbf{v}}_w^h \cdot \mathbf{n}) \right) \cdot \|\nabla\phi^h\| \, d\Omega = \int_{\Omega^h} \mathbf{v}_w^h \cdot \mathbf{c} \cdot \|\nabla\phi^h\| \, d\Omega + \int_{\partial\Omega_{N,w}^h} \mathbf{v}_w^h \cdot \hat{\mathbf{m}}_{\partial\Gamma} \cdot (\mathbf{q} \cdot \mathbf{m}) \cdot \|\nabla\phi^h\| \, d\partial\Omega. \quad (24)$$

The discrete function spaces  $\mathcal{S}_u$ ,  $\mathcal{V}_u$ ,  $\mathcal{S}_w$ , and  $\mathcal{V}_w$ , respectively, are defined as usual in the FEM. The reader is referred to [10] for further details.

## 5 NUMERICAL RESULTS

Before the presentation of some numerical test cases, error measures are introduced. The *residual errors* are obtained for the force equilibrium,  $\varepsilon_F$ , and for the moment equilibrium,  $\varepsilon_M$ , respectively. The approximated solutions  $\mathbf{u}^h$  and  $\mathbf{w}^h$  are inserted in Eqs. (21) and (22). Provided that the solution is sufficiently smooth, the errors are computed as

$$\varepsilon_F^2 = \sum_{i=1}^{n_{\text{el}}} \int_{\Omega^{\text{el},i}} \mathbf{r}_F(\mathbf{u}^h, \mathbf{w}^h) \cdot \mathbf{r}_F(\mathbf{u}^h, \mathbf{w}^h) \cdot \|\nabla\phi\| \, d\Omega, \quad (25)$$

$$\varepsilon_M^2 = \sum_{i=1}^{n_{\text{el}}} \int_{\Omega^{\text{el},i}} \mathbf{r}_M(\mathbf{u}^h, \mathbf{w}^h) \cdot \mathbf{r}_M(\mathbf{u}^h, \mathbf{w}^h) \cdot \|\nabla\phi\| \, d\Omega. \quad (26)$$

The residuals of force and moment equilibrium are defined as

$$\begin{aligned} \boldsymbol{\tau}_F(\mathbf{u}^h, \mathbf{w}^h) &= \operatorname{div}_\Gamma \mathbf{n}_\Gamma^{\text{real}}(\mathbf{u}^h, \mathbf{w}^h) + \mathbf{Q} \cdot \operatorname{div}_\Gamma \mathbf{q}_\Gamma(\mathbf{u}^h, \mathbf{w}^h) \\ &\quad + \mathbf{H} \cdot (\mathbf{q}_\Gamma(\mathbf{u}^h, \mathbf{w}^h) \cdot \mathbf{n}) + \mathbf{f}(\mathbf{x}), \end{aligned} \quad (27)$$

$$\boldsymbol{\tau}_M(\mathbf{u}^h, \mathbf{w}^h) = \mathbf{P} \cdot \operatorname{div}_\Gamma \mathbf{m}_\Gamma(\mathbf{u}^h, \mathbf{w}^h) - \mathbf{q}_\Gamma(\mathbf{u}^h, \mathbf{w}^h) \cdot \mathbf{n} + \mathbf{c}(\mathbf{x}). \quad (28)$$

A further error measurement used in this section is the *stored energy error*, obtained by

$$\varepsilon_\epsilon = \left| \boldsymbol{\epsilon}(\mathbf{u}) - \boldsymbol{\epsilon}(\mathbf{u}^h) \right|, \quad (29)$$

with the stored (elastic) energy of the Reissner–Mindlin shell defined as

$$\boldsymbol{\epsilon}(\mathbf{u}) = \frac{1}{2} \int_\Omega [\boldsymbol{\epsilon}_{\Gamma, \text{Mem}}^P(\mathbf{u}) : \tilde{\mathbf{n}}_\Gamma + \boldsymbol{\epsilon}_{\Gamma, \text{Bend}}^P(\mathbf{u}, \mathbf{w}) : \mathbf{m}_\Gamma + \boldsymbol{\epsilon}_\Gamma^S(\mathbf{u}, \mathbf{w}) : \mathbf{q}_\Gamma] \cdot \|\nabla \phi\| \, d\Omega. \quad (30)$$

This stored energy error is not to be mixed up with the classical energy error norm, see [14, 17].

### 5.1 Trigonometric shell geometry with Navier support

The geometry of this test case is from Section 5.5 in [10], but the mechanical quantities used here are different. The shell geometry is described by the level sets of the level-set function  $\phi(\mathbf{x}) = z - 2 \cdot \sin\left(\frac{1}{4} \cdot x \cdot y\right)$  and the spherical bulk domain is defined with a prescribed interval of  $\phi$  as  $\Omega = \{\mathbf{x} \in \mathbb{R}^3 : \psi(\mathbf{x}) = \|\mathbf{x}\| - 1 \leq 0 \text{ and } -\frac{1}{5} < \phi(\mathbf{x}) < \frac{2}{5}\}$ . The thickness of each shell is  $t = 0.1$ , Young’s modulus is  $E = 2.1 \cdot 10^7$ , and the applied force is  $f_z = -1000$  (acting downwards). All other applied force components, i.e.,  $f_x = f_y = 0$ , and the moment vector are zero. The whole boundary is considered as Navier supports. Fig. 5 shows the geometric setup and results for this test case. The ansatz functions for the displacement test and trial functions is one order higher than those of the difference vector. This is identified as a *mixed approach*, while we say that an *isoparametric approach* is used when the same order is applied for all test and trial functions for displacements and the difference vector, respectively. Figs. 5(c) and (d) show optimal higher-order convergence rates for the residual errors of the force and slightly sub-optimal ones of the moment equilibrium. We refer to [10] for more details.

### 5.2 Cupola with Navier support

The geometry, material parameters, and loading for this test case is from section 5.7 in [10]. Herein, the spherical shells (cupolas) are supported by Navier supports instead of clamped supports as in [10] and the isoparametric approach is used. This example shows how the simultaneous solution can be used in a design value search. The solution is obtained for all embedded shells. As a post-processing step, the geometry for which a sought target value ( $u_t$ ) is reached, is evaluated. Herein, the radius for the cupola with a maximum displacement of  $u_t = 0.045$  m at the apex is  $r_t = 9.018$  m. For a more detailed description of the design value search and comparison with a clamped support of the cupolas, we refer to [10]. Also for this example, higher-order convergence rates are obtained in the residual errors but not shown for brevity. Fig. 6 shows the geometric setup and the solution of the design value search.

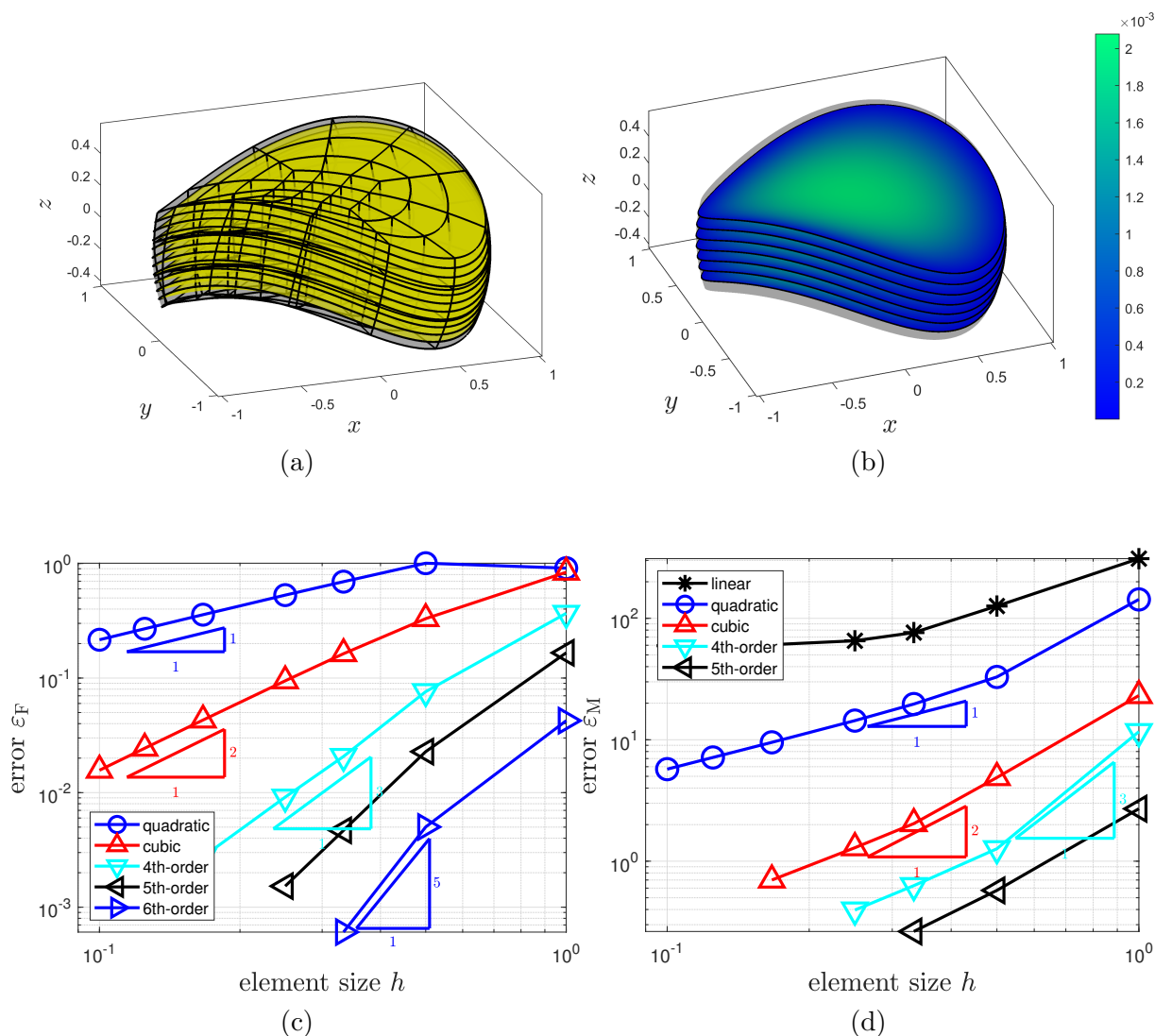


Figure 5: (a) shows the geometry with a possible discretization and some level-sets in yellow, (b) shows the Euclidean norm of the displacements, (c) the results of the convergence study for the residual error of the force equilibrium, and (d) of the moment equilibrium.

### 5.3 Influence of curvature

Numerical tests for Reissner–Mindlin shells and Timoshenko beams show that for relatively flat geometries or geometries which contain relatively flat parts, i.e., where the mean curvature goes to zero, problems occur when the isoparametric approach is used. In contrast, when the mixed approach is applied instead, the convergence rates in the stored energy error are as expected. This behaviour is illustrated in Fig. 7. The left column shows the test case of Section 5.1 with clamped support instead of Navier support: In Fig. 7(a), the mean curvature and then the higher-order convergence rates in the stored energy error  $\varepsilon_e$  for the isoparametric approach,

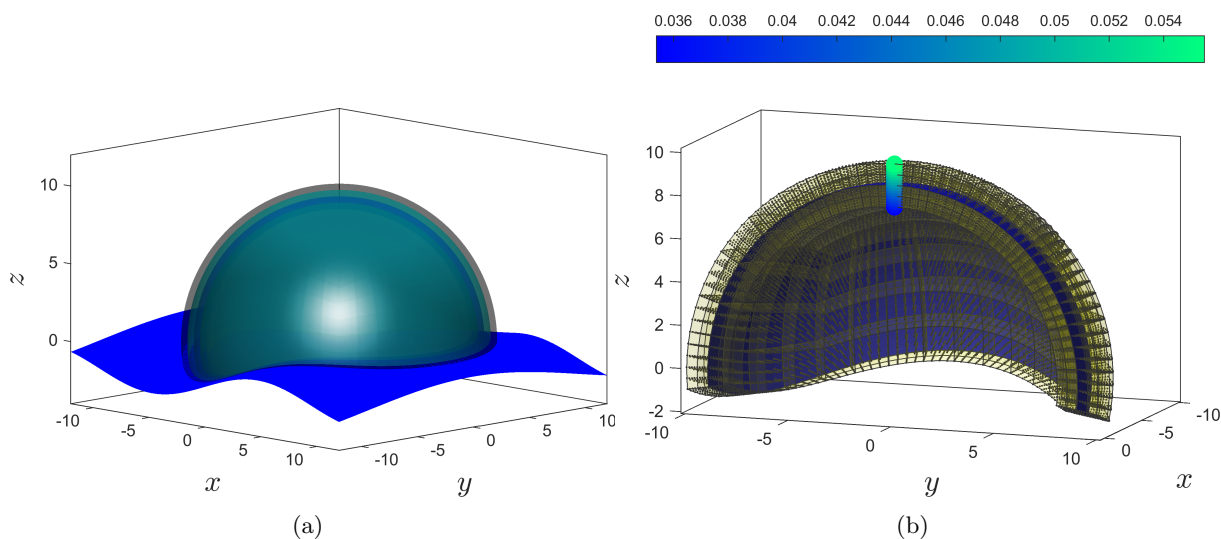


Figure 6: (a) The geometric setup of the cupola with some level sets and the curved surface which generates the boundary in dark blue. (b) Result of the design value search shown on one half of the geometry. The blue surface is the found cupola corresponding to the sought target value.

in Fig. 7(c), and for the mixed approach, in Fig. 7(e), are shown. Analogously, the right column shows the results for the test case discussed in Section 5.6 in [10]. This comparison shows that for the case of spherical shells (right column) the mixed *and* the isoparametric approach lead to optimal convergence, while for the case where the mean curvature vanishes in parts of the shell, only the mixed approach converges optimal.

## 6 Conclusions and outlook

A mechanical model and finite element method for the simultaneous analysis of Reissner–Mindlin shells is presented. The shells are modelled by level sets of a level-set function which are embedded in a three-dimensional bulk domain. For the formulation of the weak form, the co-area formula is applied. The concept can easily be adopted to curved Timoshenko beams which is a dimensional reduction by 1 of the shell counterpart.

Further research is the application of this approach in the design value search, as already outlined in one of the presented numerical test cases for a simple example, and the application in anisotropic material models reinforced with shells.

## REFERENCES

- [1] Bařar, Y. and Krätzig, W.B. 1985. *Mechanik der Flächentragwerke*. Vieweg + Teubner Verlag, Braunschweig.
- [2] Bischoff, M., Ramm, E., and Irslinger, J. 2017. “Models and Finite Elements for Thin-Walled Structures.” In *Encyclopedia of Computational Mechanics Second Edition*, edited by E. Stein, R. Borst, and T.J. Hughes. Wiley, Chichester. <http://doi.org/10.1002/9781119176817.ecm2026>

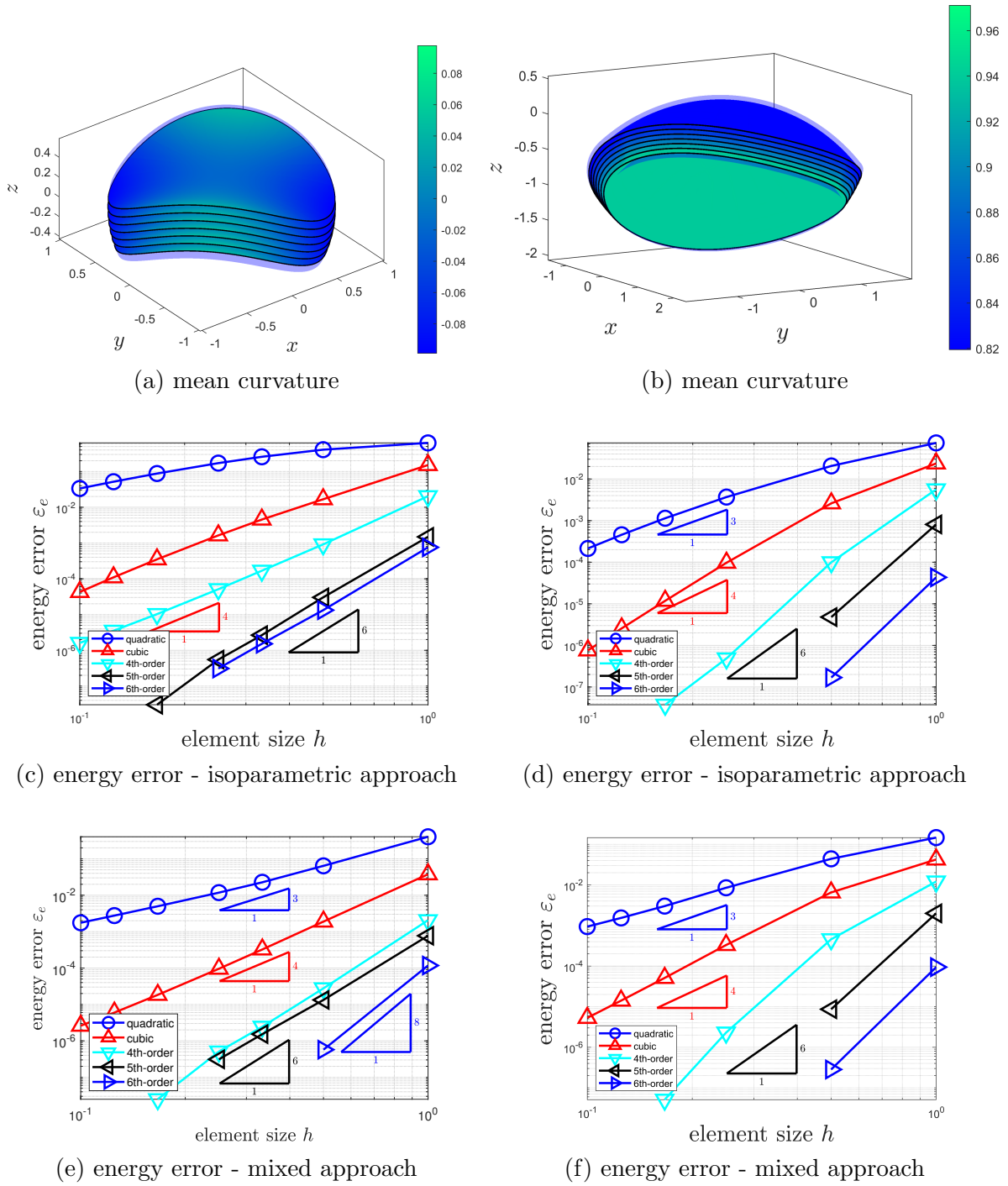


Figure 7: The influence of curvature on the convergence rates of the stored energy error. The second row shows the results for the *isoparametric* approach and the third row for the *mixed* approach. The columns refer to two different test cases. This comparison shows that the curvature is an important quantity to decide if the isoparametric approach can be applied or a mixed one is preferred.

- [3] Schöllhammer, D. and Fries, T.P. 2019. “Kirchhoff–Love shell theory based on tangential differential calculus.” *Comput Mech* 64. <http://doi.org/10.1007/s00466-018-1659-5>
- [4] Schöllhammer, D. and Fries, T.P. 2019. “Reissner–Mindlin shell theory based on tangential differential calculus.” *Comp Methods Appl Mech Engrg* 352. <http://doi.org/10.1016/j.cma.2019.04.018>
- [5] Hansbo, P., Larson, M.G., and Larsson, K. 2014. “Variational formulation of curved beams in global coordinates.” *Comput Mech* 53. <http://doi.org/10.1007/s00466-013-0921-0>
- [6] Kaiser, M.W. and Fries T.P. 2023. “Curved, linear Kirchhoff beams formulated using tangential differential calculus and Lagrange multipliers.” *Proc Appl Math Mech* 22. <http://doi.org/10.1002/pamm.202200042>
- [7] Fries, T.P. and Schöllhammer, D. 2020. “A unified finite strain theory for membranes and ropes.” *Comp Methods Appl Mech Engrg* 365. <http://doi.org/10.1016/j.cma.2020.113031>
- [8] Delfour, M.C. and Zolésio, J.P. 2011. *Shapes and geometries: metrics, analysis, differential calculus, and optimization*. SIAM.
- [9] Schöllhammer D. and Fries, T.P. 2021. “A higher-order Trace finite element method for shells.” *Internat J Numer Methods Engrg* 122. <http://doi.org/10.1002/nme.6558>
- [10] Kaiser, M.W. and Fries, T.P. 2024. “Simultaneous analysis of continuously embedded Reissner-Mindlin shells in 3D bulk domains.” *Internat J Numer Methods Engrg* early online view. <http://doi.org/10.1002/nme.7495>
- [11] Kaiser, M. and Fries, T.P. 2024. “Simultaneous solution of implicitly defined curved, linear Timoshenko beams in two-dimensional bulk domains.” *Proc Appl Math Mech*, submitted.
- [12] Dziuk, G., Elliott, C. 2013. “Finite element methods for surface PDEs.” *Acta Numer* 22. <http://doi.org/10.1017/s0962492913000056>
- [13] Burger, M. (2009). “Finite element approximation of elliptic partial differential equations on implicit surfaces.” *Comput Vis Sci* 12. <http://doi.org/10.1007/s00791-007-0081-x>
- [14] Fries, T.P. and Kaiser, M.W. 2023. “On the simultaneous solution of structural membranes on all level sets within a bulk domain.” *Comp Meth Appl Mech Engrg* 415. <http://doi.org/10.1016/j.cma.2023.116223>
- [15] Kaiser, M.W. and Fries, T.P. 2023. “Simultaneous solution of ropes and membranes on all level sets within a bulk domain.” *Proc Appl Math Mech* John 23. <http://doi.org/10.1002/pamm.202300035>
- [16] Fries, T.P. and Kaiser, M.W. 2023. “The Bulk Trace FEM for the simultaneous solution of structural membranes on all level sets over a bulk domain.” *Proc Appl Math Mech* 23. <http://doi.org/10.1002/pamm.202300028>
- [17] Zienkiewicz, O., Taylor, R. and Zhu, J. 2013. *The Finite Element Method: Its Basis & Fundamentals*, vol. 7. Butterworth-Heinemann, Oxford.